Synchronous Condenser Placement for Multiple HVDC Power Systems Considering Short-Circuit Ratio Requirements

Jiaxin Wang, *Graduate Student Member, IEEE*, Jiawei Zhang, *Graduate Student Member, IEEE*, Qingchun Hou, *Member, IEEE*, and Ning Zhang, *Senior Member, IEEE*

***Abstract*—High voltage direct current (HVDC) power injections decrease power systems' short-circuit ratio (SCR) and the grid strength. They may cause voltage stability problems, especially in systems with a high share of renewable. The synchronous condenser (SynCon) is a promising solution for increasing the SCR. However, planning SynCons to meet the SCR requirements is challenging since the SCR requirement is a set of nonlinear eigenvalue inequality constraints that are not friendly to solvers. Based on generalized spectral decomposition, this paper proposes a Rayleigh cut method to equivalently transform eigenvalue inequality constraints into a set of linear constraints. Then, a mixed-integer linear programming model is built to solve the SCR-constrained SynCon placement problem. The proposed approach's convergence, complexity, and error analysis are all analyzed theoretically. Also, numerical comparisons with the other seven models suggest the proposed model is effective and efficient, outperforming the other models in terms of solution quality and computation time.**

***Index Terms*—Synchronous condenser placement, short-circuit ratio, eigenvalue inequality constraint, Rayleigh cut constraint.**

NOMENCLATURE

Abbreviations

HVDC	High Voltage Direct Current.
SynCon	Synchronous Condenser.
VRE	Variable Renewable Energy.
SCR	Short-Circuit Ratio.
UC	Unit Commitment.
MLP	Multilayer Perceptron.
LP	Linear Programming.
MILP	Mixed Integer Linear Programming.
SDP	Semidefinite Programming.
MISDP	Mixed Integer Semidefinite Programming.

Math Operators

$\lambda(\cdot)$	Eigenvalue set of a matrix.
$\lambda(\cdot,*)$	Generalized eigenvalue set of two matrices
$\det(\cdot)$	Determinant of a matrix.
$\cdot \succeq 0, \cdot \succ 0$	Positive (semi-)definite matrix.
$\|\cdot\|_2$	2-norm of a vector or a matrix.
$\|\cdot\|_P$	P-norm of a vector, given $P \succ 0$
$\|\cdot\|_\infty$	Infinity norm of a vector or a matrix.
$\mathrm{vec}(\cdot)$	Vectorization of a matrix.
$\mathrm{diag}(\cdot)$	Diagonal matrix with the input vector on its diagonal.
$.^{\mathrm{T}}$	Transpose of a matrix or a vector
$\|\cdot\|$	Cardinality of a set or absolute value.

Variables

x	On/off binary decisions of generators.
χ	SynCon placement binary decisions.
P	Diagonal matrix with the corresponding HVDC rate power on its diagonal.
B_r, B	(Reduced) admittance matrix.
γ_0, γ	(Required) short-circuit ratio.
u	Rayleigh cut vectors.
h	Number of HVDC terminals.
d	Total number of generators and SynCons.

I. INTRODUCTION

THE voltage stability under highly penetrated renewable is a critical issue for modern power systems, especially when multiple high voltage direct current (HVDC) converters are connected. In China, more than 20 cross-regional HVDCs carry green power from inland to coastal areas, and the number continues to increase [1], [2], [3]. As a result, both the sending-end system's grid strength and the receiving-end system's grid strength are significantly weakened by HVDCs. Moreover, the highly penetrated variable renewable energy (VRE) sources and HVDC injections significantly replace the local thermal generators, the main contributors to the system grid strength. The grid strength is insufficient to support some voltage drops caused by disturbances that should have been allowed to occur occasionally [4], [5], [6]. Therefore, enhancing the grid strength is necessary to ensure system security.

The short-circuit ratio (SCR) was initially used to measure system grid strength with a single HVDC connection [7]. For

Manuscript received 10 October 2023; revised 16 January 2024 and 14 April 2024; accepted 19 May 2024. Date of publication 22 May 2024; date of current version 27 December 2024. This work was supported by Carbon Neutrality and Energy System Transformation Project initiated by Tsinghua University. Paper no. TPWRS-01600-2023. *(Corresponding author: Ning Zhang.)*

Jiaxin Wang, Jiawei Zhang, and Ning Zhang are with the State Key Laboratory of Power Systems, Department of Electrical Engineering, Tsinghua University, Beijing 100084, China (e-mail: jiaxinwangthu@gmail.com; zhang-jw19@mails.tsinghua.edu.cn; ningzhang@tsinghua.edu.cn).

Qingchun Hou is with Alibaba Group, Hangzhou 310000, China (e-mail: qingspring@outlook.com).

Color versions of one or more figures in this article are available at https://doi.org/10.1109/TPWRS.2024.3404116.

Digital Object Identifier 10.1109/TPWRS.2024.3404116

systems with multiple HVDC connections, the SCR is generalized [8], [9]. First, a series of empirical indices are proposed to assess the grid strength of systems with multiple HVDC connections. The most well-known of these empirical indices is the multi-infeed short-circuit ratio (MISCR), which can be used to calculate an equivalent SCR value at each HVDC terminal [8]. The empirical indices are easy to understand, but they lack mathematical rigor. Therefore, some theoretical indices are proposed. Among these indices, the generalized short-circuit ratio (GSCR) is the most widely used one [9]. The advantages of the GSCR are at least twofold. First, it is shown that the MISCR can be derived from the GSCR, given some particular assumptions. In this sense, the MISCR is a particular case of the GSCR. Second, the GSCR has the same threshold/critical value as the traditional SCR. This property enables the GSCR to be used similarly to the traditional SCR. Therefore, this paper uses the GSCR to assess the grid strength. Without ambiguity, we will write SCR instead of GSCR for the rest of this paper.

Installing synchronous condensers (SynCons) is a promising solution to enhance the SCR. The advantages of SynCons are at least twofold. First, SynCons can provide reactive power and inertia to support the system [10]. The reactive power output of SynCons can even reach 200% to 350% of its rated power, which is almost irrelevant to the system voltage. In contrast, the reactive power output of static var compensators (SVCs) is inversely proportional to the square of the system voltage [11]. The reactive power output of static synchronous compensators (STATCOMs) is inversely proportional to the system voltage [12]. In addition, SynCons can provide a large amount of reactive power support immediately after a disturbance occurs due to its advanced exciter system [13]. Second, SynCons can be reconstructed from retired thermal generators, which is economical. A case study in Australia [14] and a case study in India [15] show that using SynCons is a cost-effective solution for improving system stability. Therefore, installing SynCons is a proper solution to enhance the SCR.

However, it is challenging to formulate the SCR requirement in the SynCon placement problem due to two obstacles. First, the SCR has no closed-form expression. It is straightforward to evaluate the SCR value given the system states. Still, it is difficult to explicitly model the SCR expression when making decisions [16]. The SCR requirement is a set of nonlinear eigenvalue inequality constraints, which are not friendly to optimization solvers. Second, the SCR is calculated based on a reduced network of all HVDC terminals [9]. The reduced admittance matrix is related to the original matrix by Gaussian elimination, which is also difficult to be expressed in optimizations [17].

Some researchers have studied the SCR enhancement problem in recent years. First, a semi-definite programming (SDP) model is proposed to determine the capacities of the supporting devices under a specific SCR requirement [18]. In their work, the locations of the supporting devices are relaxed to be continuous decisions, and the SCR requirement is formulated as an SDP constraint. Second, a mixed-integer semi-definite programming (MISDP) model is proposed to determine the locations of the supporting devices under a specific SCR requirement [19]. In their work, the locations of the supporting devices are not relaxed but modeled as binary decisions, and the SCR requirement is formulated as an MISDP constraint. System operations, such as the unit commitment (UC), are not considered in either work. However, the UC results severely affect the SCR value since the UC determines the on/off status of synchronous generators, which contribute significantly to SCR via their dynamic impedance. Then, a mixed-integer second-order cone programming (MISOCP) model is proposed to determine the UC results when preventing the system operations from the voltage collapse [20]. Moreover, a SOCP formulation is used to model the SCR requirement. The SOCP formulation can only prevent the system operations from voltage collapse. Still, it cannot maintain the system SCR above a given threshold. The correlation between the admittance/impedance matrix and the binary decisions of the generators' on/off status is fitted through a quadratic regression. However, quadratic regression may introduce too many additional binary decisions in the optimization model, increasing the computational burden.

We built an MILP model to solve the SCR-constrained SynCon placement problem. First, we proposed a data-driven method to express the nonlinear reduced admittance variables as mixed-integer linear expressions. Second, we proposed a Rayleigh cut method to mathematically model the eigenvalue inequality SCR requirement into a set of cut planes. Combining the above two methods, we reformulated the nonlinear SCR requirement into a set of mixed-integer linear constraints. Then, the SCR-constrained SynCon placement problem is formulated as an MILP model. We provide a detailed theoretical discussion of the proposed model's convergence, complexity, and error analysis. In case studies, different models are compared regarding the computational burden and the effectiveness of the SCR constraints. The results suggest the proposed model is effective and efficient, consistent with the theoretical analysis.

The major contributions of this paper are summarized as follows.

- We built an MILP model to solve the SCR-constrained SynCon placement problem, which is effective and easy for commercial solvers.
- We proposed a Rayleigh cut method to model the nonlinear SCR requirement mathematically. This method provides a general solution for handling the eigenvalue inequality constraints in optimizations.
- We proposed a data-driven method to express the nonlinear reduced admittance variables as mixed-integer linear expressions. An error analysis is conducted to theoretically bound the impact of the approximation error in a reasonable range.

The remainder of this paper is organized as follows. In Section II, the motivations of this study and our solution are presented. In Section III, a data-driven method is proposed to model the nonlinear reduced admittance variables into mixed-integer linear constraints. In Section IV, a Rayleigh cut method is proposed to equivalently reformulate the SCR requirement into a set of linear constraints. In Section V, an MILP model is built to solve the SCR-constrained SynCon placement problem. In Section VI, some practical issues of the proposed model are discussed theoretically, including the set value of the big

M and the error analysis of the data-driven method. Finally, in Section VII, the effectiveness of the proposed model is verified through case studies, and the results are discussed.

II. Motivations and Our Solution

A. Motivations

The short-circuit ratio (SCR) reflects the grid strength of a power system. As the renewable and the HVDC injections increase, the system SCR becomes insufficient. On the other hand, the synchronous condenser (SynCon) is widely deployed as a mature technique to enhance the system SCR for weak-strength systems. This paper determined where and how many SynCons should be placed in power systems with high renewable penetration and HVDC integration. We solved a placement model by minimizing the operation and investment costs considering SCR requirements. Since the SCR is primarily determined by the on/off status of various synchronous generators and condensers, it is necessary to derive the mathematical constraints for SCR requirements and embed them into the optimization model.

The nonlinearity of the SCR is the main obstacle to integrating the SCR requirement into the SynCon placement problem. We need to develop an efficient approach to model this requirement in optimizations. Let γ be the generalized SCR of a system with multiple HVDC terminals [9], then,

$$\gamma := \min \lambda(-P^{-1}B_r). \tag{1}$$

P is a constant diagonal matrix with the diagonal entries of each HVDC's nominal power capacity, i.e., $P = \mathrm{diag}(P_1, \ldots, P_h)$, where h is the number of HVDCs. B_r is the reduced admittance matrix after Kron reduction is performed, with only HVDC terminals being reserved. Appendix E gives an example to illustrate the meaning of B_r. $\lambda(-P^{-1}B_r)$ is the eigenvalue set of Matrix $-P^{-1}B_r$.

Generally, the SCR requirement is given by a threshold γ_0, i.e.,

$$\gamma = \min \lambda(-P^{-1}B_r) \geq \gamma_0. \tag{2}$$

However, inequality (2) cannot be directly integrated into optimizations due to its high nonlinearity from the following two aspects.

First, the value of the Kron-reduced admittance matrix B_r is correlated with the binary values of the generators' on/off decision variable x and SynCons' placement decision variable χ. The correlation is nonlinear for the following reasons. Suppose that B is the original admittance matrix, then,

$$B_{ij} = \begin{cases} -b_{ij}, & i \neq j \\ b_i^G x_i + b_i^C \chi_i + \sum_{k \in i} b_{ik}, & i = j \end{cases}, \tag{3}$$

where b_{ij} is the admittance of Branch (i, j), b_i^G is the admittance of the generator at Bus #i and b_i^C is the admittance of the SynCon at Bus #i. The off-diagonal elements of B are constant, while the diagonal elements are linear to x and χ as shown in (3). We divide B into blocks according to buses with HVDC terminals (labeled as H) and the remaining buses (labeled as L).

$$B = B(x, \chi) = \begin{bmatrix} B_{HH}(x, \chi) & B_{HL} \\ B_{LH} & B_{LL}(x, \chi) \end{bmatrix}, \tag{4}$$

where the diagonal elements of B_{HH} and B_{LL} are linearly related to x and χ, while the other elements are constant. Then, the reduced admittance matrix B_r is calculated as

$$B_r = B_r(x, \chi) = B_{HH}(x, \chi) - B_{HL}B_{LL}(x, \chi)^{-1}B_{LH}. \tag{5}$$

The inverse operation introduces nonlinearity into $B_r(x, \chi)$.

Second, the eigenvalue set $\lambda(-P^{-1}B_r)$ and the minimum eigenvalue $\min \lambda(-P^{-1}B_r)$ are nonlinear to B_r because the eigenvalues of a matrix usually cannot be linearly expressed by its entries in most cases. A trivial approach that can be implemented to tackle this nonlinearity is to use the semi-definite reformulation technique. Applying this technique, (2) can be equivalently expressed as a semi-definite programming (SDP) constraint:

$$P^{-1}B_r + \gamma_0 I \preceq 0 \Leftrightarrow B_r + \gamma_0 P \preceq 0, \tag{6}$$

where I is the identity matrix with a suitable size, and $\cdot \preceq 0$ means non-positive definite. Binary variables are imported to describe B_r, so the resulting SynCons placement problem turns into a mixed-integer semi-definite programming (MISDP) problem. A heavy computational burden of solving MISDP problems is usually inevitable. Therefore, we must develop a solver-friendly method to model the SCR requirement.

In summary, the nonlinear admittance $B_r = B_r(x, \chi)$ and the nonlinear eigenvalue $\gamma = \min \lambda(-P^{-1}B_r)$ result in the nonlinearity of the SCR requirement (2).

B. Our Solution

In Section III, we proposed a data-driven multi-layer perceptron (MLP) to learn the nonlinear admittance $B_r = B_r(x, \chi)$. Then, we formulated the correlation between B_r and x, χ as a set of mixed-integer linear expressions.

In Section IV, we derived a Rayleigh cut method to model the nonlinear SCR inequality $\gamma = \min \lambda(-P^{-1}B_r) \geq \gamma_0$ as a set of Rayleigh cuts $u^{\mathrm{T}}B_r u \leq -\gamma_0$. Since u is constant and B_r has linear expressions based on the work in Section III, the Rayleigh cuts are mixed-integer linear constraints.

In Section V, we built an MILP model (23)–(32) to solve the complete SCR-constrained SynCon placement problem. An iterative procedure for solving the problem is proposed.

III. Formulation of The Reduced Admittance Matrix

This section proposes an efficient data-driven method to formulate the reduced admittance matrix $B_r(x, \chi)$ in the SynCon placement problem. Moreover, we analyze the complexity of the proposed method and compare it with the existing approach.

A. Explicit Admittance Formulation

The nonlinearity of (5) comes from the inverse operation $B_{LL}(x,\chi)^{-1}$. By introducing auxiliary decisions and reformulating the constraints, the nonlinear $B_{LL}(x,\chi)^{-1}$ can be equivalently linearized by a set of mixed-integer linear constraints.

Let $Z = B_{LL}^{-1}$, then $B_{LL}Z = I$, i.e.,

$$\begin{cases} \sum_k B_{h+i,h+k} Z_{k,j} = 1, & i = j \\ \sum_k B_{h+i,h+k} Z_{k,j} = 0, & i \neq j \end{cases}, \tag{7}$$

where $h := |H|$ is the scale of B_{HH}. Combining (7) with (3), we see that the nonlinearity of (7) only comes from the products $x_{h+i}Z_{ij}$ and $\chi_{h+i}Z_{ij}$ for all $i,j \in \{1,2,\ldots,|L|\}$. Let $z_{ij}^G = x_{h+i}Z_{ij}$ and $z_{ij}^C = \chi_{h+i}Z_{ij}$, then, the nonlinearity of $B_{LL}(x,\chi)^{-1}$ is equivalently transformed into these two products.

The nonlinear product equations $z_{ij}^G = x_{h+i}Z_{ij}$ and $z_{ij}^C = \chi_{h+i}Z_{ij}$ both involve the product of a binary decision and a continuous decision. Take $z_{ij}^G = x_{h+i}Z_{ij}$ for example. It can be equivalently transformed into the following set of mixed-integer linear constraints.

$$\begin{cases} z_{ij}^G = x_{h+i}Z_{ij} \\ \underline{Z_{ij}} \le Z_{ij} \le \overline{Z_{ij}} \\ x_{h+i} \in \{0,1\} \end{cases} \Leftrightarrow \begin{cases} z_{ij}^G \le \overline{Z_{ij}} x_{h+i} \\ z_{ij}^G \ge \underline{Z_{ij}} x_{h+i} \\ z_{ij}^G \le \overline{Z_{ij}} - \underline{Z_{ij}}(1 - x_{h+i}) \\ z_{ij}^G \ge Z_{ij} - \overline{Z_{ij}}(1 - x_{h+i}) \\ x_{h+i} \in \{0,1\} \end{cases} \tag{8}$$

where $\overline{Z_{ij}}, \underline{Z_{ij}}$ are the upper and lower bounds of Z_{ij} respectively. The final equivalent formulation in (8) is a set of mixed-integer linear expressions. The product $\chi_{h+i}Z_{ij}$ can be equivalently represented similarly. Combining (5) and (7)–(8), the reduced admittance matrix B_r is linearized as a set of mixed-integer linear expressions.

However, the explicit admittance expressions (5) and (7)–(8) introduce massive additional decisions and constraints. Suppose the total dimension of x, χ is d; it introduces $\mathcal{O}(2\,d^2)$ additional decision variables and $\mathcal{O}(5\,d^2)$ additional constraints. A comprehensive analysis is presented in Section III-C.

B. Data-Driven Admittance Formulation

The explicit admittance expressions (5) and (7)–(8) are computationally expensive. In this subsection, we propose a fine-tuned multi-layer perceptron (MLP) model to reformulate the correlation between B_r and x, χ into the MILP.

The fine-tuned MLP model is shown in Fig. 1. First, we pre-train a classic MLP with ReLu activations to learn the nonlinear correlation between $B_{HL}B_{LL}(x,\chi)^{-1}B_{LH}$ and x, χ. Second, we set all coefficients ($W^{(k)}$ and $b^{(k)}$) with absolute values less than 1×10^{-3} for all neurons to zero. This step is indispensable when embedding the model into optimizations since those small values may result in a bad numerical condition for the problems. Third, we remove the output layer and re-train a lasso regression layer (the linear head) instead. This step compensates for the additional error caused in the previous step. Finally, we obtain a fine-tuned MLP model whose coefficients contribute a good condition number for the target optimization problems. The normalization of the output is used in the proposed fine-tuned MLP model.

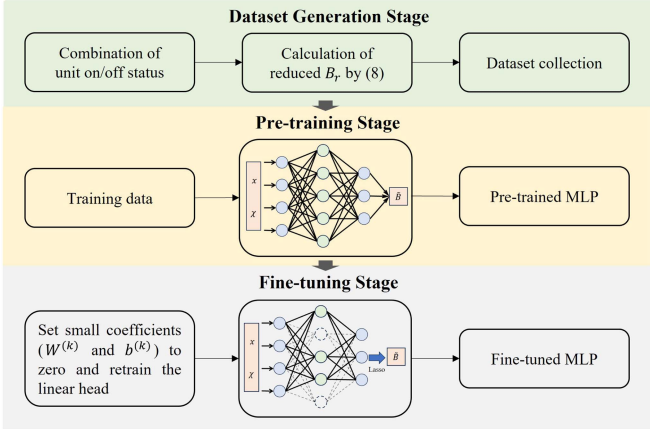

Fig. 1. The training procedure for fine-tuned MLP model.

We embed the fine-tuned MLP model into optimizations. For convenience, we denote $B_{HL}B_{LL}^{-1}B_{LH}$ by $\tilde{B}$. The following represents the correlation between $\tilde{B}$ and x, χ by the fine-tuned MLP model.

$$\begin{cases} y^{(1)} = \max\left\{ W^{(1)} \begin{bmatrix} x \\ \chi \end{bmatrix} + b^{(1)}, 0 \right\}, \\ y^{(k)} = \max\left\{ W^{(k)} y^{(k-1)} + b^{(k)}, 0 \right\}, \ 2 \le k \le K-1, \\ \mathrm{vec}(\tilde{B}) = W^{(K)} y^{(K)} + b^{(K)}, \end{cases} \tag{9}$$

where $\mathrm{vec}(\tilde{B})$ reshapes Matrix $\tilde{B}$ into a long vector, $W^{(k)}$ and $b^{(k)}$ are the weights and biases of the k-th layer respectively, and K is the number of layers.

Then, (9) is equivalently transformed into the following MILP formulation using the big-M method.

$$\begin{cases} y^{(0)} := \begin{bmatrix} x \\ \chi \end{bmatrix}, \\ y^{(k)} \ge W^{(k)} y^{(k-1)} + b^{(k)}, \\ y^{(k)} \le W^{(k)} y^{(k-1)} + b^{(k)} + M(1 - z^{(k)}), \\ 0 \le y^{(k)} \le M z^{(k)}, \\ z^{(k)} \in \{0,1\}, \\ k = 1, 2, \ldots, K-1, \\ \mathrm{vec}(\tilde{B}) = W^{(K)} y^{(K)} + b^{(K)}, \end{cases} \tag{10}$$

where M is a large constant number.

As for the structure of the fine-tuned MLP model, we set the number of Layers K to 3. Then, the proposed fine-tuned MLP model (10) introduces only $\mathcal{O}(2\,d)$ additional decision variables and $\mathcal{O}(8\,d)$ additional constraints. A comprehensive analysis is presented in Section III-C.

C. Complexity Analysis

In this subsection, we analyze the complexity of the proposed admittance formulation (10) and compare it with the explicit expressions (5) and (7)–(8).

The number of decisions and constraints can roughly measure the complexity of the MILP. Suppose B_{LL} is of size $n > d$. The explicit formulation (7)–(8) introduces n^2 decisions Z_{ij} and n^2 constraints, as well as dn products $x_g Z_{ij}$ and $x_c Z_{ij}$. Each product introduces one additional decision and four additional constraints. Thus, the explicit formulation introduces $n(n+d) > 2\,d^2$ additional decisions and $n(n+4\,d) > 5\,d^2$ additional constraints. However, the proposed formulation (10) only introduces $2\,d$ neurons. Each neuron introduces one additional decision and four additional constraints. Thus, the proposed formulation introduces $2\,d$ additional decisions and $8\,d$ additional constraints. Here, the number of constraints $\mathrm{vec}(\tilde{B}) = W^{(K)} y^{(K)} + b^{(K)}$ is ignored, since the size of $\tilde{B}$ is much smaller than n. In summary, the number of additional introduced decisions and constraints of the explicit formulation is quadratic to the dimension of the decisions x, χ, while the number of the proposed formulation is linear. Therefore, the complexity of the proposed formulation (10) is much lower than that of the explicit formulation (7)–(8).

IV. Derivation of SCR Constraints

In this section, we equivalently derive a set of linear constraints, named Rayleigh cuts, from the SCR requirement (2). The convergence of the proposed Rayleigh cuts is also analyzed. The Rayleigh cut method is first proposed in this paper to model the eigenvalue inequality SCR requirement (2) as a set of linear constraints. Inspired by the Rayleigh quotient in Courant-Fischer theorem [21], the authors of this paper give the name of the Rayleigh cut.

A. Reformulation of the SCR Requirement

In this subsection, the SCR requirement (2) is reformulated into a set of linear constraints.

First, suppose α is an eigenvalue of $-P^{-1}B_r$, then α satisfies

$$\det(\alpha I + P^{-1}B_r) = \det(P^{-1})\det(\alpha P + B_r) = 0. \quad (11)$$

Since $P \succ 0$, we have $\det(P^{-1}) \neq 0$. Thus, α can be equivalently obtained by

$$\det(\alpha P + B_r) = 0. \quad (12)$$

Equation (12) is the definition of the generalized eigenvalue set $\lambda(-B_r, P)$, i.e., $\alpha \in \lambda(-B_r, P)$ for all α satisfying (12). The corresponding generalized eigenvector u is the solution of the following equation.

$$-B_r u = \alpha P u,\ u \neq 0. \quad (13)$$

Thus, the SCR γ can be equivalently calculated as follows.

$$\gamma = \min \lambda(-P^{-1}B_r) = \min \lambda(-B_r, P). \quad (14)$$

Second, the smallest generalized eigenvalue of $(-B_r, P)$ can be equivalently calculated by (15), which is illustrated by Theorem 1.

$$\gamma = \min \lambda(-B_r, P) = \min_{\|u\|_P = 1} -u^{\mathrm{T}} B_r u. \quad (15)$$

Theorem 1: Suppose that $P \succ 0$ is diagonal and that B_r is symmetric. Then,

$$\min \lambda(-B_r, P) = \min_{\|u\|_P = 1} -u^{\mathrm{T}} B_r u, \quad (16)$$

where $\|\cdot\|_P$ is a vector norm induced by the positive-definite diagonal matrix P, i.e., $\|u\|_P = \sqrt{u^{\mathrm{T}} P u}$.

Proof: Since $P \succeq 0$ is diagonal, there is a diagonal matrix $\sqrt{P} \succeq 0$ such that $P = \sqrt{P}^2$. Then, we obtain $\lambda(-B_r, P) = \lambda(-\sqrt{P}^{-1} B_r \sqrt{P}^{-1})$.

According to the Courant-Fischer theorem [21],

$$\begin{aligned} \min \lambda(-B_r, P) &= \min \lambda(-\sqrt{P}^{-1} B_r \sqrt{P}^{-1}) \\ &= \min_{\|y\|_2 = 1} -y^{\mathrm{T}} \sqrt{P}^{-1} B_r \sqrt{P}^{-1} y \\ &= \min_{\|u\|_P = 1} -u^{\mathrm{T}} B_r u. \end{aligned} \quad (17)$$

The proof is completed. □

Therefore, the SCR requirement (2) can be equivalently expressed as

$$\gamma = \min_{\|u\|_P = 1} -u^{\mathrm{T}} B_r u \geq \gamma_0, \quad (18)$$

which is also equivalent to

$$u^{\mathrm{T}} B_r u \leq -\gamma_0, \quad \forall u \in U := \{u \mid \|u\|_P = 1\}. \quad (19)$$

B. Procedure of Generating and Adding Rayleigh Cuts

The set U in (19) is infinite, but we can construct a finite subset $\overline{U} \subset U$ to equivalently replace U in (19) since the possible values of $B_r = B_r(x, \chi)$ are finite.

$$\overline{U} = \left\{ u \,\middle|\, \begin{matrix} -B_r(x,\chi)u = \alpha P u,\ \forall x, \chi,\ \exists \alpha \in \mathbb{R} \\ \|u\|_P = 1 \end{matrix} \right\}. \quad (20)$$

The finite set $\overline{U}$ is composed of the related generalized eigenvectors of $(-B_r(x,\chi), P)$.

Then, the original nonlinear SCR constraint (2) is equivalently transformed into a set of linear constraints (21) as follows.

$$u^{\mathrm{T}} B_r u \leq -\gamma_0, \quad \forall u \in \overline{U}. \quad (21)$$

Although (21) is a finite set of linear constraints, it is unnecessary to add all constraints into the SynCon placement problem at once. We propose an algorithm to iteratively add effective constraint $u^{\mathrm{T}} B_r u \leq -\gamma_0$ until the SCR requirement (2) is satisfied when the optimal solution is reached. Each constraint $u^{\mathrm{T}} B_r u \leq -\gamma_0$ is named a Rayleigh cut.

The algorithm is shown in Algorithm 1.

The proposed procedure of adding Rayleigh cuts is convergent and effective. Whenever the feasible decisions cannot satisfy the SCR requirement, the related Rayleigh cut is added as an active constraint, which cuts off a nonempty decision region from the original region. Section IV-C shows the algorithm has a quadratic convergence rate.

Algorithm 1: Generating and Adding Rayleigh Cuts.

Input: $\gamma_0 > 0$, $P \succ 0$
Output: Rayleigh cuts $Cons$, $\tilde{U}$
Initialization: SynCon placement problem $Problem$ without SCR requirement
$[x, \chi] \leftarrow$ optimal decisions from $Problem$
$B_r \leftarrow B_r(x, \chi)$ by (5)
$[\gamma, u] \leftarrow$ smallest generalized eigenpair of $(-B_r, P)$
while $\gamma < \gamma_0$ **do**
  $u \leftarrow u/\|u\|_P$
  $\tilde{U} \leftarrow \tilde{U} \cup \{u\}$
  $Cons \leftarrow Cons \cup \{u^{\mathrm{T}} B_r(x, \chi) u \le -\gamma_0\}$
  $Problem \leftarrow Problem \cup Cons$
  $[x, \chi] \leftarrow$ optimal decisions from $Problem$
  $B_r \leftarrow B_r(x, \chi)$ by (5)
  $[\gamma, u] \leftarrow$ smallest generalized eigenpair of $(-B_r, P)$
end while
return $Cons$

C. Convergence Analysis

In this subsection, we analyze the convergence of Algorithm 1. First, we show that the algorithm terminates in finite steps. Second, we show that the algorithm has a quadratic convergence rate to the error.

The algorithm terminates in finite steps. Although the algorithm has many possible early termination conditions, we only analyze the worst case. Suppose that the minimum generalized eigenpair of $(-B_r(x, \chi), P)$ is $(\gamma(x, \chi), u(x, \chi))$ with $\|u(x, \chi)\|_P = 1$. Then, the worst case is that the algorithm terminates when $\tilde{U}$ expands to $\overline{U}$. Since x, χ are binary decisions, the number of possible $u(x, \chi)$ values is finite. In each iteration, the algorithm adds at least one $u(x, \chi)$ from $\overline{U}$ into $\tilde{U}$. Thus, the algorithm terminates in finite steps.

The algorithm has a quadratic convergence rate to the error. This argument is based on Theorem 2.

Theorem 2: Suppose $\tilde{U}$ is a finite set composed of some vectors u satisfying $\|u\|_P = 1$. Then,

$$\min_{u \in \tilde{U}} | - u^{\mathrm{T}} B_r u - \gamma| \le \mathcal{O}(\epsilon^2),\ \epsilon := \mathrm{dist}(u^*, \tilde{U}), \tag{22}$$

where $\mathrm{dist}(\cdot)$ is the Euclidean distance between a vector and a set of vectors, u^* is the target vector satisfying $-u^{*\mathrm{T}} B_r u^* = \gamma$ and $\|u^*\|_P = 1$.

Proof: The proof is shown in Appendix A. □

Therefore, Algorithm 1 is complete and efficient. The generated Rayleigh cuts can be used to thoroughly and efficiently formulate the SCR requirement (2) in the SynCon placement problem.

V. Synchronous Condenser Placement Model

A. Basic Settings

In this subsection, we introduce the basic settings of the SynCon placement problem.

Multiple scenarios are considered in this paper. We collect a dataset of load profiles and renewable generations based on our previous work [22], [23]. Then, we apply the k-medoids clustering algorithm to obtain typical scenarios to constitute a scenario set $\mathcal{S}$ with their corresponding probability weights w_s for all $s \in \mathcal{S}$. We choose typical days to constitute a scenario set $\mathcal{S}$ with $|\mathcal{S}|$ scenarios. For each Scenario $s \in \mathcal{S}$, the time horizon $\mathcal{T}$ is divided into $|\mathcal{T}|$ time intervals, each of which is one hour. At every time interval $t \in \mathcal{T}$ of each Scenario $s \in \mathcal{S}$, the load forecast and the renewable generation forecast are given as the input of the placement model. The linear power flow model is adopted, which is widely used in power system operation and planning [24], [25]. We clarify that other power flow models, such as the second-order cone programming (SOCP) power flow model [26] and the semi-definite programming (SDP) power flow model [27], can also be used in our SynCon placement model if necessary and computable. In Section VII-D2, we conduct a numerical experiment to show the validity of those convex AC power flow models in our SynCon placement model. However, a more detailed discussion on power flow models is beyond the scope of this paper. Synchronous generators, synchronous condensers, and grid-forming converters are modeled as voltage sources, which provide positive contributions to the SCR; while grid-following converters are modeled as current sources that are assumed to have no contribution to the SCR.

The SynCon placement problem can be viewed as a MILP problem. The objective comprises the investment cost of SynCons and the operation cost.

B. Placement Model

The objective is to minimize the total cost Obj as follows:

$$\begin{aligned} Obj = &\sum_{c \in \mathcal{C}} \mathrm{CI}_c \chi_c + \sum_{g \in \mathcal{G}} \sum_{s \in \mathcal{S}} w_s \sum_{t \in \mathcal{T}} (\mathrm{CF}_g x_{g,s,t} \\ &+ \mathrm{CV}_g p_{g,s,t} + \mathrm{CSU}_g s u_{g,s,t} + \mathrm{CSD}_g s d_{g,s,t}) \\ &+ \sum_{n \in \mathcal{N}} \sum_{s \in \mathcal{S}} w_s \sum_{t \in \mathcal{T}} \mathrm{CP}_n (\Delta \bar{p}_{n,s,t} + \Delta \bar{q}_{n,s,t}). \end{aligned} \tag{23}$$

The first term is the investment cost of SynCons, where CI_c is the investment cost of SynCon $c \in \mathcal{C}$ and χ_c is the binary variable indicating whether the SynCon is installed. The investment cost CI_c has been converted to match the time horizon $\mathcal{T}$ according to the annualized interest rate. The second term is the operation cost of generators, where CF_g, CV_g, CSU_g, and CSD_g are the fixed cost, the variable cost, the startup cost, and the shutdown cost of Generator $g \in \mathcal{G}$, respectively. The binary variables $x_{g,s,t}$, $su_{g,s,t}$ and $sd_{g,s,t}$ indicate whether Generator g is on, startup, and shutdown at Time t of Scenario s, respectively. The variable $p_{g,s,t}$ is the active power output of Generator g at Time t of Scenario s. The third term is the penalty cost of nodal power imbalance, where CP_n is the penalty cost of nodal power imbalance at Bus $n \in \mathcal{N}$. The variables $\Delta \bar{p}_{n,s,t}$ and $\Delta \bar{q}_{n,s,t}$ are the active and reactive power imbalance at Bus n at Time t of Scenario s, respectively. The scenario probability is denoted by w_s.

The power flow constraints are given by

$$\begin{bmatrix}\bar{p}_{s,t}\\ \bar{q}_{s,t}\end{bmatrix}+\begin{bmatrix}\Delta\bar{p}_{s,t}\\ \Delta\bar{q}_{s,t}\end{bmatrix}=\mathrm{DLPF}\begin{bmatrix}\theta_{s,t}\\ v_{s,t}\end{bmatrix}, \tag{24}$$

where $\bar{p}_{s,t}, \bar{q}_{s,t}$ are the active and reactive nodal power injection vectors, $\Delta\bar{p}_{s,t}, \Delta\bar{q}_{s,t}$ are the active and reactive power imbalance vectors, and $\theta_{s,t}, v_{s,t}$ are the voltage angle vector and voltage magnitude vector, respectively. The detailed expression of DLPF can be found in [24]. The nodal power injections $\bar{p}_{s,t}$ and $\bar{q}_{s,t}$ are equal to the sum of generator injections, load injections, HVDC injections, and SynCon injections. The vector form constraints are given by

$$\bar{p}_{s,t}=p_{s,t}+p_{s,t}^{\mathrm{Load}}+p_{s,t}^{\mathrm{HVDC}}, \tag{25a}$$

$$\bar{q}_{s,t}=q_{s,t}+q_{s,t}^{\mathrm{Load}}+q_{s,t}^{\mathrm{HVDC}}+q_{s,t}^{\mathrm{SynCon}}, \tag{25b}$$

where $p_{s,t}$ and $q_{s,t}$ are the generator active and reactive power injections; $p_{s,t}^{\mathrm{Load}}$ and $q_{s,t}^{\mathrm{Load}}$ are the load active and reactive power injections; $p_{s,t}^{\mathrm{HVDC}}$ and $q_{s,t}^{\mathrm{HVDC}}$ are the HVDC active and reactive power injections; $q_{s,t}^{\mathrm{SynCon}}$ is the SynCon reactive power injections. Besides, the SynCon reactive power injections are constrained by the corresponding placement decision χ.

$$\underline{Q}_c\chi_c\le q_{c,s,t}^{\mathrm{SynCon}}\le\overline{Q}_c\chi_c, \tag{26}$$

where $\underline{Q}_c$ and $\overline{Q}_c$ are the minimum and maximum reactive power output of SynCon $c\in\mathcal{C}$, respectively.

The unit commitment (UC) constraints given by [28] are adopted in this paper. They are composed of decision variable bound constraints, generator on-off status constraints, minimum startup and shutdown time constraints, and ramping constraints.

The bound constraints are as follows:

$$P_g^{\min}x_{g,s,t}\le p_{g,s,t}\le P_g^{\max}x_{g,s,t}, \tag{27a}$$

$$Q_g^{\min}x_{g,s,t}\le q_{g,s,t}\le Q_g^{\max}x_{g,s,t}, \tag{27b}$$

where $P_g^{\min}$ and $P_g^{\max}$ are the minimum and maximum power output of Generator $g\in\mathcal{G}$, respectively; $Q_g^{\min}$ and $Q_g^{\max}$ are the minimum and maximum reactive power output of Generator $g\in\mathcal{G}$, respectively.

The generator on-off status constraints are as follows:

$$x_{g,s,t}-x_{g,s,t-1}=su_{g,s,t}-sd_{g,s,t}. \tag{28}$$

The minimum startup and shutdown time constraints are as follows:

$$x_{g,s,t}\ge\sum_{\tau=t-T_g^{\mathrm{on}}+1}^{t}su_{g,s,\tau} \tag{29a}$$

$$x_{g,s,t}\le 1-\sum_{\tau=t-T_g^{\mathrm{off}}+1}^{t}sd_{g,s,\tau}, \tag{29b}$$

where T_g^{on} and T_g^{off} are the minimum start-up and shut-down time of Generator $g\in\mathcal{G}$, respectively.

The ramping constraints are as follows:

$$p_{g,s,t}-p_{g,s,t-1}\le R_gx_{g,s,t-1}+R_g^{\mathrm{SU}}su_{g,s,t}, \tag{30a}$$

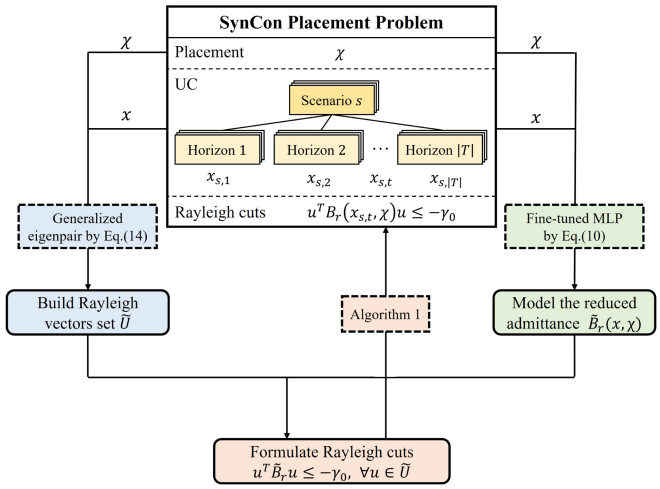

Fig. 2. Procedure of solving the placement model.

$$p_{g,s,t-1}-p_{g,s,t}\le R_gx_{g,s,t}+R_g^{\mathrm{SD}}sd_{g,s,t}, \tag{30b}$$

where R_g is the ramping limit of Generator g; R_g^{SU} and R_g^{SD} are startup capacity and shutdown capacity of Generator $g\in\mathcal{G}$, respectively.

Besides, the bus voltage magnitude constraints are given by

$$V_n^{\min}\le v_{n,s,t}\le V_n^{\max}, \tag{31}$$

where $V_n^{\min}$ and $V_n^{\max}$ are the minimum and maximum voltage magnitude of Bus $n\in\mathcal{N}$, respectively.

Finally, the SCR constraints are as follows:

$$\begin{aligned}&u^{\mathrm{T}}B_r(x_{s,t},\chi)u\le-\gamma_0, && \forall u\in\overline{U},\\ &(5),\ (10), && \forall s\in\mathcal{S},\forall t\in\mathcal{T},\end{aligned} \tag{32}$$

The SCR constraints are iteratively added to the placement model until the SCR requirements are satisfied.

C. Procedure for Solving the Placement Model

The procedure for solving the SCR-constrained placement model is shown in Fig. 2.

First, a SynCon placement problem without the SCR requirement is formulated by the objective (23), power flow equations (24) and operation constraints (25)–(31). An MILP solver is used to solve the problem.

Second, the SCR values are evaluated for every time interval t of every Scenario s based on the current solution by (5) and (14). The procedure terminates if the SCR requirements (2) are satisfied at every time interval t of every Scenario s.

Otherwise, the SCR requirements are violated at some time interval t of some scenario s. The Rayleigh cut vectors are calculated based on the current value of $(x_{s,t},\chi)$ by (13). The constraint (10) is added into the placement problem to model the reduced admittance matrix $B_r(x_{s,t},\chi)$.

Then, the Rayleigh cuts are generated and added to the placement problem by Algorithm 1. The placement problem is solved again by the solver.

Finally, we repeat steps from the second to the fourth until the SCR requirements for all time intervals of all scenarios are satisfied.

VI. Discussions

This section discusses four details of the proposed approach. First, we show the bounds of Z_{ij} in (8) exist and give an explicit formula to calculate them in practice. Second, we derive a formula for the set value of M in the big-M method. Third, we analyze the SCR error caused by the proposed MLP model to show that the error is acceptable in practice. Finally, we give an accuracy analysis of the Rayleigh cut method.

A. Explicit Formula for the Bounds of Z_{ij}

The nonlinear product $x_{h+i}Z_{ij}$ (or similarly $\chi_{h+i}Z_{ij}$) constraints can be equivalently represented by a set of linear constraints, as shown in (8). However, the upper and lower bounds of Z_{ij} are not given. We must guarantee these bounds exist and can be straightforwardly calculated in practice.

In this subsection, we show that the upper and lower bounds exist and give an explicit formula (33) to determine the bounds $\overline{Z_{ij}}, \underline{Z_{ij}}$ in practice.

$$-\kappa\|B_{LL}^0\|_\infty^{-1} \le Z_{ij} \le \kappa\|B_{LL}^0\|_\infty^{-1},\ \forall i,j=1,2,\dots,n. \quad (33)$$

where $B_{LL}^0 := B_{LL}(0,0)$ is the corresponding admittance matrix without considering the units' admittance and the SynCons' admittance, n is the size of B_{LL}, and κ is a constant that is independent of the decision variables. Theorem 3 demonstrates this inequality. The detailed formula of κ is also derived in the proof.

Theorem 3: Partition $B_{LL}(x,\chi) = B_{LL}^0 + D(x,\chi)$, where $D(x,\chi)$ is a diagonal matrix with the diagonal entries being $b_i^G x_i + b_i^C \chi_i$. Let $Z = Z(x,\chi) = B_{LL}(x,\chi)^{-1}$, then the (i,j) element of Z is bounded, i.e.,

$$\max_{i,j} |Z_{ij}| \le \kappa\|B_{LL}^0\|_\infty^{-1}, \quad (34)$$

where κ is independent of x and χ.

Proof: The proof is given in Appendix B. □

Theorem 3 gives an explicit formula of the upper and lower bounds of Z_{ij}. Therefore, we have shown that the equivalent expression (8) is valid in practice. In our test system, the bound $\kappa\|B_{LL}^0\|_\infty^{-1} \approx 20.5$, which is in the reasonable range and would not cause numerical issues in practice. In this paper, we set the bound of Z_{ij} as 25 in case studies.

B. The Set Value for M in the Big-M Method

From (9) to (10), the proposed MLP model is equivalently transformed into a set of MILP constraints using the big-M method. Theoretically, the value of M can be arbitrarily large. But in practice, a too-large value of M will lead to numerical issues and low efficiency. In this subsection, we derive an explicit formula for the lower bound of M.

$$M := \max_{1\le k\le K} M_k, \quad (35)$$

where

$$M_k := \prod_{i=1}^{k} \|W^{(i)}\|_\infty + \sum_{i=1}^{k} \|b^{(i)}\|_\infty \prod_{j=i+1}^{k} \|W^{(j)}\|_\infty. \quad (36)$$

The detailed derivation is given in Appendix C.

Note that the normalization of the output does not affect the derivation of the formula for M. Combining (36) and (35), we can obtain a reasonable value of M. In our numerical experiments, the calculated value of M equals 22.24. In this paper, we set $M = 30$ in case studies.

C. Error Analysis of B_r on the SCR

Errors are inevitable for all data-driven approaches and numerical methods. The key lies in how much the error caused by the proposed MLP model will affect the SCR value.

In this subsection, we derive a detailed error analysis to demonstrate the impacts of the error caused by the proposed approach. Suppose B_r and γ are the actual values of the reduced admittance matrix and the related SCR, respectively, and $\tilde{B}_r$ and $\tilde{\gamma}$ are the corresponding approximations obtained by the proposed approach. We want to discuss how much error of γ will be caused by the error of B_r. The conclusion is that the SCR error $\tilde{\gamma} - \gamma$ is bounded by the admittance error $\delta := \max_{i,j} |\tilde{B}_{r,ij} - B_{r,ij}|$, i.e.,

$$|\tilde{\gamma} - \gamma| \le \frac{\sum_{i,j} \sqrt{P_i P_j}^{-1} |y_i y_j|}{y^{\mathrm{T}} y} \delta + o\left(\delta^2\right), \quad (37)$$

where y is the eigenvector of $-\sqrt{P}^{-1} B_r \sqrt{P}^{-1}$ corresponding to γ, and P_i is the diagonal entry of P. This conclusion is presented in the proof of Theorem 4.

Theorem 4: The SCR error $|\tilde{\gamma} - \gamma|$ is bounded by the admittance error $\delta := \max_{i,j} |\tilde{B}_{r,ij} - B_{r,ij}|$ as shown in inequality (37).

Proof: The proof is given in Appendix D. □

Theorem 4 shows that the SCR error $\tilde{\gamma} - \gamma$ is bounded by the admittance error δ. The coefficient $C := \frac{\sum_{i,j} \sqrt{P_i P_j}^{-1} |y_i y_j|}{y^{\mathrm{T}} y}$ in (37) reflects the sensitivity of the SCR to the admittance error. Numerical experiments show that C is small enough. In our test system, the mean value of C is around 0.2908, and the standard deviation is around 0.0019. Also, the admittance error δ caused by the proposed fine-tuned MLP model is small. The mean value of δ is around 0.02, and the standard deviation is around 0.01. Therefore, the SCR error caused by the data-driven fine-tuned MLP model is less than 10^{-2}, which is acceptable in practice.

Moreover, we point out that the result of the error analysis is just an upper bound of the SCR error. The actual SCR error caused by the proposed MLP model is even smaller than the upper bound. The actual error is represented in Fig. 4. The perturbed value $\tilde{\gamma}$ is very close to the actual value γ. The numerical result is also consistent with the theoretical analysis.

D. Accuracy of the Rayleigh Cut Method

Rayleigh cut method, first proposed in this paper, reformulates the nonlinear SCR requirement $\lambda(-P^{-1}B_r(x,\chi)) \ge \gamma_0$ into a

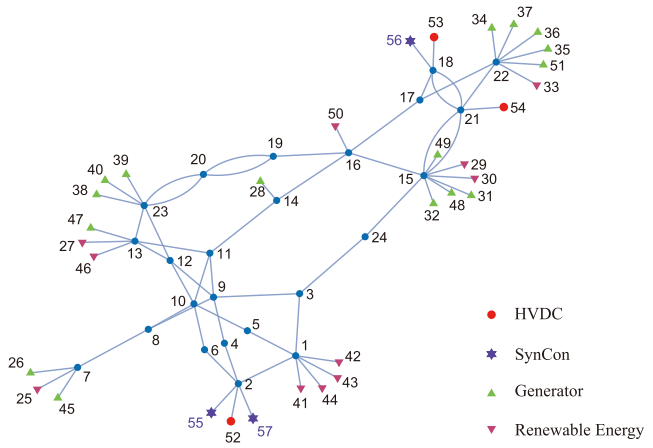

Fig. 3. Network and placement results. The blue nodes represent buses, the blue edges represent transmission lines or transformers, the red nodes represent HVDC terminals, the upward green triangles represent generators, the downward pink triangles represent renewable energy sources, and the purple star represents the placed SynCons.

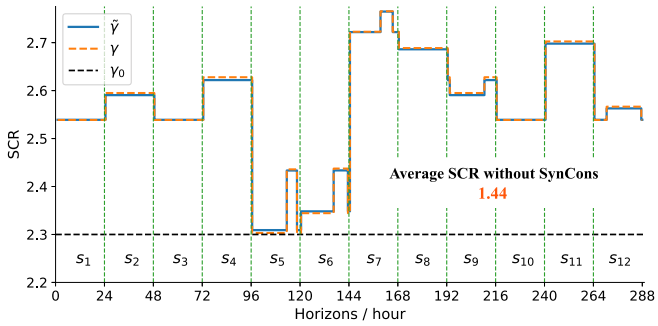

Fig. 4. SCR resulting from the proposed model. The blue line represents the approximate SCR $\tilde{\gamma}$ evaluated based on the approximate B_r with the proposed fine-tuned MLP. The orange dashed line represents the real SCR γ. The black dashed line represents the SCR requirement γ_0. For convenience, the 12 scenarios are pieced together along the x-axis, with the green dashed lines indicating the boundaries of the scenarios.

set of linear constraints in (32). Each constraint in (32), called a Rayleigh cut, is a linear constraint $u^{\mathrm{T}} B_r(x,\chi)u \le -\gamma_0$ to decision variable B_r. The reformulation itself is exact and does not introduce any approximation error. We have shown it in Section IV. However, the relationship $B_r = B_r(x,\chi)$ is modeled by (5) and (10), which introduce approximation errors. The approximation error caused by (5) and (10) is analyzed in Section VI-C, where a theoretical upper bound of the SCR error is derived. Therefore, the accuracy of the Rayleigh cut method is guaranteed theoretically. Besides, numerical experiments are also conducted in Section VII, suggesting that the accuracy is acceptable in practice.

VII. Case Studies

A. Data Description

We use a modified IEEE-RTS79 system as the test system. The system has 24 buses, 38 transmission lines, 3 HVDC terminals, 11 renewable energy sources, and 16 synchronous generators. All the sources are connected to the grid through transformers or lines, modeled as branches with the corresponding tap ratio and angle shift. The system is drawn in Fig. 3, where the blue nodes represent buses, the blue edges represent transmission lines or transformers, the red nodes represent HVDC terminals, the upward green triangles represent generators, and the downward pink triangles represent renewable energy sources. The three HVDC terminals are connected to Bus #2, Bus #18, and Bus #21. The transmission capacities of these HVDCs are 1200 MW, 1000 MW, and 900 MW, respectively. The capacity of the synchronous condenser to be installed is 300 MVar, and the transient impedance is 0.3 p.u. based on its capacity. A synchronous condenser's total investment cost is 160 million Chinese Yuan (CNY), and the annualized investment cost rate is set to 0.19. The investment cost data is sourced from a real engineering project in China. In addition, three types of generators are considered. The capacity, transient impedance, minimum on/off time, minimum technique power, and cost coefficients of the three types of generators are given in Table I. The total load demand is 6465 MW on average. The total capacity of VREs is 2200 MW, and the annual capacity utilization hour is 1957 hours on average.

TABLE I
Generator Types

	Type 1	Type 2	Type 3
Capacity (MW)	667	600	300
X'_d (p.u.)[1]	0.040	0.045	0.089
Min On Time (h)	10	10	4
Min Off Time (h)	18	16	6
Min Power (p.u.)[2]	0.40	0.35	0.30
CF (kCNY/h) [3]	1.70	1.50	1.00
CV (kCNY/MWh)	0.15	0.20	0.25
CSU (kCNY)	250	200	100
CSD (kCNY)	50	30	20

[1] per unit value based on 100 MVA.
[2] per unit value based on its capacity.
[3] kCNY is short for a thousand Chinese Yuan.

The rest of this section is organized as follows. In Section VII-B, the placement result of the proposed SynCon placement model is presented. In Section VII-C, the placement results of the proposed model are validated in other scenarios. In Section VII-D1, the proposed admittance formulation is compared with other typical methods. In Section VII-D2, the proposed placement model is compared with other models.

The codes in this section are finished in Python 3.10 and Matlab R2022b. Optimization problems are solved by Gurobi 10.0 [29] (for MILP problems) and MOSEK 10.0 [30] (for SDP problems). Specifically, MISDP problems are solved using the branch-and-bound method with SDP solver MOSEK 10.0. The computation is performed on an AMD-RT-5950X CPU.

B. Placement Results

In this subsection, we present the result of the proposed SynCon placement model.

Fig. 3 shows the whole network, including the placement result of SynCons. Three 300 MW SynCons are placed, with one SynCon placed at Bus #18 and the other two SynCons placed at Bus #2. The placement result is understandable. We see three

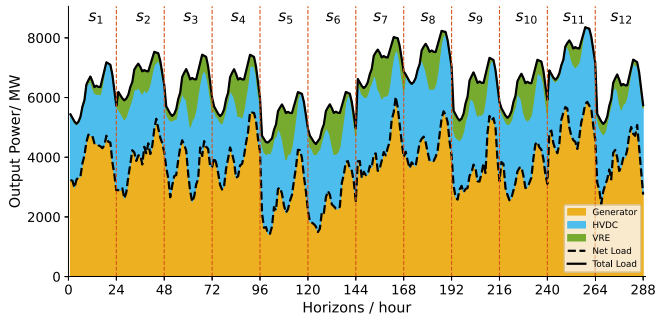

Fig. 5. Operation results of the placement model.

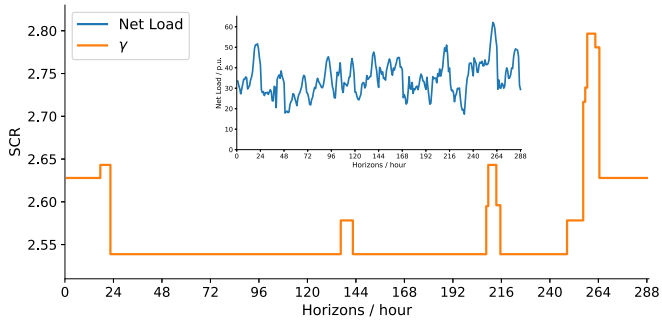

Fig. 6. SCR evaluation in other conditions. The subfigure drawn in blue shows the net load curve, which differs from the previous one.

reasons why two SynCons are placed at Bus #2. First, the HVDC with the largest capacity, 1200 MW, is connected to Bus #2. Second, Bus #2 is close to Bus #1, to which three current sources are connected. Third, Bus #2 is far from voltage sources, and the neighboring buses are all load buses. The abovementioned conditions make Bus #2 important for SCR improvement. Thus, our model places two SynCons at Bus #2. We also see three reasons for the placement of the other SynCon. First, the HVDC with the second largest capacity, 1000 MW, is connected to Bus #18, and the third HVDC is very close to Bus #18. Thus, the system may need a SynCon at Bus #18 to improve the SCR. Second, compared to Bus #2, Bus #18 is closer to the voltage sources, so the SynCon number at Bus #18 may be less than that at Bus #2. Third, there are more voltage sources around Bus #21 than around Bus #18, so the SynCon may be placed at Bus #18 instead of Bus #21. In addition, since Bus #21 is very close to Bus #18, the SynCon at Bus #18 may also support Bus #21. As a result, one SynCon is placed at Bus #18 in our model.

Fig. 4 shows the SCR evaluation of the system with the placed SynCons in different scenarios. The SCR requirement is set to 2.3 according to the engineering practice. The blue line represents the approximate SCR $\tilde{\gamma}$ evaluated during the optimization stage based on the approximate B_r with the proposed fine-tuned MLP (10). The orange dashed line represents the real SCR γ evaluated after the optimization. The numerical results indicate the two following conclusions. First, The real SCR requirement is satisfied in all scenarios. No violation occurs in any horizon. Second, the relative error measured by the root mean square value between $\tilde{\gamma}$ and γ is 0.14%, which is consistent with the error analysis in Section VI-C. Moreover, the average SCR without SynCons is 1.44, and the average SCR with SynCons is 2.57. The system SCR is increased by 1.13 on average. We see that the reasonable placement of SynCons improves the system SCR, demonstrating the validity of the proposed model. In addition, combined with the net load demand shown in Fig. 5, the system strength tends to decrease when the net load demand decreases. The low net load demand reduces the number of online generators, causing the system to be more vulnerable to disturbances.

C. Validations of the Placement Results

In this subsection, we validate the placement result of the proposed model in other scenarios. First, we place the SynCons in the system according to the placement result of the proposed model. Second, we randomly generate another 12 scenarios, which differ from those used in the proposed SynCon placement model. The net load is shown in the subfigure of Fig. 6. Third, based on the generated conditions, we solve the corresponding UC problem to simulate the system's operation with the placed SynCons. The UC problem includes the SynCons planned by the proposed model and excludes the SCR requirement constraint (32). Then, we evaluate the SCR in each horizon, which is shown in Fig. 6. From Fig. 6, we see that the SCR requirement is satisfied in all horizons, demonstrating that the proposed model's placement result is valid in other scenarios. Also, we may conclude that the numerical validation suggests a good coverage of our selected scenarios.

TABLE II
RMSE ERROR ON TEST SET

	$B_{r,11}$[1]	$B_{r,12}$[2]	$B_{r,22}$	$B_{r,13}$	$B_{r,23}$	$B_{r,33}$
MLP	**2.80E-4**	**1.46E-4**	**1.64E-4**	**2.12E-4**	**2.42E-4**	**3.85E-4**
LR	2.80E-3	1.51E-3	2.35E-3	1.68E-3	2.60E-3	2.90E-3
QR	7.30E-4	3.57E-4	4.36E-4	5.06E-4	6.18E-4	8.81E-4
SVR	2.92E-3	1.60E-3	2.53E-3	1.78E-3	2.81E-3	3.14E-3
DT	3.20E-3	3.46E-3	3.82E-3	5.02E-3	5.66E-3	8.39E-3
ResNet	4.23E-4	1.46E-4	1.50E-4	2.13E-4	2.11E-4	3.36E-4
CNN	1.09E-3	4.79E-4	6.46E-4	7.48E-4	1.01E-3	1.62E-3

[1] per unit value based on 100 MVA.
[2] E-3 is short for $\times 10^{-3}$ and E-4 is short for $\times 10^{-4}$.

D. Discussions

1) Accuracy of the Admittance Formulation: We compare the proposed admittance formulation (9) with other typical methods, including linear regression (LR), quadratic regression (QR), support vector regression (SVR) with linear kernel, decision tree (DT) with a depth of no more than six, residual neural network (ResNet) with eight layers, and convolutional neural network (CNN) with eight layers. The neuron number in a hidden layer of the ResNet / CNN is set to 64. The kernel size of the convolutional layer of the CNN is set to 3. We use accurate Gaussian elimination as the baseline. The size of the training set is 58982 samples, and the size of the test set is 6554. The root-mean-square error (RMSE) is used as a metric to measure the accuracy of the approximation methods. The comparison results are shown in Table II, where the proposed fine-tuned

MLP is abbreviated as MLP for short. Due to the symmetric property, we only show the results of the upper triangular part of B_r.

Table II suggests that the proposed method accurately approximates B_r. In detail, the accuracy of the proposed method is an order of magnitude higher than that of the LR, SVR, and DT methods. The accuracy of the QR is also slightly lower than that of the proposed method. These comparison results demonstrate that $B_r(x, \chi)$ in (5) cannot be accurately approximated by a linear function due to its nonlinearity. Nonlinear models such as QR, CNN, ResNet, and the proposed MLP model can capture the nonlinearity well.

The proposed method has a significant advantage when considering the corresponding computational efficiency in optimizations. Although the QR method has an accuracy similar to the proposed method, the quadratic approximation of B_r may lead to a high computational burden in the corresponding optimizations. As analyzed in Section III-C, the proposed fine-tuned MLP only introduces d additional continuous decisions, d auxiliary binary decisions, and $8\,d$ additional constraints, while the QR method needs to introduce $d(d-1)/2$ auxiliary binary decisions and $3d(d-1)/2$ additional constraints. The computational burden introduced by the proposed method is much lower than that of the QR method. Similarly, a deeper DT may give better accuracy than the current DT. However, it will also introduce a higher computational burden proportional to its depth's exponential degree. As for the CNN, the convolutional operation is complex to embed into MILP optimizations. Although the ResNet can be embedded into MILP optimizations using the same technique as the proposed method, it uses eight layers of over 400 neurons, which is much more complex than the proposed method, of which the number of neurons is just less than 35. It should be noted that our target is not to achieve the highest accuracy but to achieve an acceptable accuracy with a low computational burden in the placement optimization model.

Therefore, the proposed fine-tuned MLP performs well in both the approximation accuracy and the introduced computational efficiency, being a suitable choice for approximating the reduced admittance matrix B_r in optimizations.

2) Comparison With Other Models: We compare the proposed placement model with the other seven models. For brevity, we name the other six models as *A*, *B*, *C*, *D*, *E*, *F*, and *G*. Model *A* replaces the fine-tuned MLP in our proposed placement model with the explicit admittance formulation (7)–(8). Model *B* replaces it with LR. Model *C* replaces it with QR. Model *D* replaces it with DT of depth 6. Model *E* replaces it with DT of depth 7. Model *F* uses the MISDP model with the SCR constraint (6). Model *G* replaces the linear power flow in the proposed placement model with the SOCP power flow. Details about the SOCP power flow can be found in [26], [31]. We set the MIP gap to 1% for all models. We set the solving time limit to 3 hours for the first five models and 10 hours for Model *F*. The MIP gap setting may be violated when the time limit is reached.

Table III shows the comparison results. Our proposed model achieves an MIP gap of less than 1% in 7.69 minutes and does not violate the SCR requirement in any horizon. The proposed model outperforms other models in both the solution quality and the computational efficiency. First, although Model *A* (using the explicit admittance formulation) is accurate, it is also time-consuming. Model *A* uses up the time limit of 3 hours but only achieves a MIP gap of 20.90%, which is far from an acceptable solution quality. The heavy computational burden of Model *A* is mainly caused by the explicit admittance formulation (7)–(8). This result is consistent with that of the analysis in Section III-C. Second, Model *B* (using LR) is the fastest model since the corresponding admittance approximation is linear but also the least accurate model. In the result of Model *B*, 48 of the 288 horizons violate the SCR requirement. The SynCons are not appropriately placed to enhance the system SCR. Third, Model *C* (using QR) is more accurate than Model *B*, but it is also time-consuming. Model *C* takes 50.83 minutes to achieve an MIP gap of less than 1%, 6.61 times longer than our proposed model. Model *D* and Model *E* embed the DT technique. The former Model *D* (depth 6) is inaccurate. In the result of Model *D*, 38 of the 288 horizons violate the SCR requirement. This result is consistent with the numerical results in Section VII-D1. However, when the depth of DT increases to 7, the computational burden of Model *E* increases dramatically. Model *E* uses up the time limit of 3 hours but does not achieve a feasible solution. The reason is that the number of introduced binary decisions by the DT is proportional to the exponential degree of its depth. Model *F* uses the MISDP model with the SCR constraint (6). It uses up the time limit of 10 hours but does not achieve a feasible solution. The reason is that the MISDP problem is much more challenging than the MILP problem. The computation burden is heavy and grows dramatically with the increasing scale of the problem. Model *G* uses the SOCP power flow instead of the linear power flow in the proposed model. Model *G* 's placement result is the same as that of the proposed model. They both place two SynCons at Bus #2 and one SynCon at Bus #18, as shown in Fig. 3. However, the computational efficiency of Model *G* is much lower than that of the proposed model. In summary, the proposed model can effectively place SynCons to enhance the system SCR and outperform other models in both solution quality and computational efficiency.

TABLE III
COMPARISON OF DIFFERENT MODELS

Model[1]	Time / min	Violation[2]	Gap[3]
This paper	**7.69**	**0**	**≤1%**
Model *A*	180	0	20.90%
Model *B*	4.83	48	≤1%
Model *C*	50.83	0	≤1%
Model *D*	28.65	38	≤1%
Model *E*	180	-	-
Model *F*	≥600	-	-
Model *G*	46.95	0	≤1%

[1] Model *A* uses the explicit admittance formulation (7)-(8); Model *B* uses LR; Model *C* uses QR; Model *D* uses DT of depth 6; Model *E* uses DT of depth 7; Model *F* uses the MISDP model with the SCR constraint (6); Model *G* is the same as the proposed model but uses the SOCP power flow instead of the linear power flow.
[2] the number of horizons in which the SCR requirement is violated.
[3] MIP gap, less than 1% by default.

VIII. Conclusion

This paper builds an MILP model to solve the SCR-constrained SynCon placement problem. The SCR requirement is nonlinear since the eigenvalue inequality is nonlinear to the reduced admittance variables, and the reduced admittance variables are nonlinear to the SynCon placement decision variables and the unit commitment decision variables. A data-driven multi-layer perceptron is used to express the nonlinear reduced admittance variables into mixed-integer linear equations. A Rayleigh cut method is proposed to turn the nonlinear eigenvalue inequality into a set of linear cut planes. The SCR requirement is reformulated into a set of mixed-integer linear constraints by combining the above two methods. Thus, the MILP placement model is built. The number of introduced additional decisions and constraints is bounded by the linear order of the number of system generators. Thus, the computational burden is acceptable and much improved compared to the previous work. In the case study, different models are compared regarding the computational burden and the effectiveness of the SCR constraints. Numerical results verify the effectiveness and efficiency of the proposed model and are consistent with the theoretical analysis.

Future work may include the following two aspects. First, the short-circuit current constraint may be included. Second, the contribution of SynCons to inertia may be considered.

Appendix

A. Proof of Theorem 2

Proof: Since $-u^{*\mathrm{T}} B_r u^* = \gamma$ and $\|u^*\|_P = 1$, we have

$$-B_r u^* = \gamma P u^*. \tag{38}$$

For any $u \in \tilde{U}$, write $\delta u := u - u^*$. We see

$$\|u\|_P = 1 = \|u^*\|_P \Rightarrow \|\delta u\|_P^2 = -2\, u^{*\mathrm{T}} P \delta u. \tag{39}$$

Then

$$\begin{aligned} |-u^{\mathrm{T}} B_r u - \gamma| &= |2\, u^{*\mathrm{T}} B_r \delta u + \delta u^{\mathrm{T}} B_r \delta u| \\ &= |2\gamma u^{*\mathrm{T}} P \delta u + \delta u^{\mathrm{T}} B_r \delta u| \\ &= |\delta u^{\mathrm{T}} B_r \delta u - \gamma \|\delta u\|_P^2| \\ &= |\delta u^{\mathrm{T}} Q^{\mathrm{T}} \Lambda Q \delta u - \gamma \|\delta u\|_P^2| \\ &\le \sum_i |\lambda(B_r)_i| (Q\delta u)_i^2 + \gamma \|\delta u\|_P^2 \\ &\le (\max |\lambda(B_r)|)\, \|\delta u\|_2^2 + \gamma \|\delta u\|_P^2 \\ &= \mathcal{O}(\|\delta u\|_2^2), \end{aligned} \tag{40}$$

where $B_r = Q^{\mathrm{T}} \Lambda Q$ is the orthogonal spectral decomposition, in which Q is orthogonal and $\Lambda = \mathrm{diag}(\lambda(B_r))$. In the derivation of (40), the second equality is due to (38), the third equality is due to (39), and the last equality can be found in [21]. Finally, we see

$$\min_{u \in \tilde{U}} |-u^{\mathrm{T}} B_r u - \gamma| \le \mathcal{O}(\min_{u \in \tilde{U}} \|\delta u\|_2^2) = \mathcal{O}(\epsilon^2). \tag{41}$$

Note that more exact bounds in (40) may be derived by other advanced scaling techniques, but the quadratic convergence rate $\mathcal{O}(\epsilon^2)$ does not change. □

B. Proof of Theorem 3

Proof: First, we present a matrix norm inequality [21]. For any square matrix A of size n,

$$\|A\|_\infty \le \sqrt{n} \|A\|_2. \tag{42}$$

Using this inequality, we see

$$\|B_{LL}^0 + D(x,\chi)\|_2 \ge \frac{1}{\sqrt{n}} \|B_{LL}^0 + D(x,\chi)\|_\infty. \tag{43}$$

Since the diagonal entries of B_{LL}^0 and $D(x,\chi)$ are non-positive, it is easy to see $\|B_{LL}^0 + D(x,\chi)\|_\infty \ge \|B_{LL}^0\|_\infty$. Thus,

$$\|B_{LL}^0 + D(x,\chi)\|_2 \ge \frac{1}{\sqrt{n}} \|B_{LL}^0\|_\infty. \tag{44}$$

Let $\sigma_1(x,\chi) \ge \ldots \ge \sigma_n(x,\chi) \ge 0$ be the singular values of $B_{LL}(x,\chi)$ and $\tau_1 \ge \ldots \ge \tau_n \ge 0$ be the singular values of B_{LL}^0. Then, the 2-norm identity implies

$$\begin{aligned} \|Z\|_2 &= \| \left(B_{LL}^0 + D(x,\chi)\right)^{-1} \|_2 \\ &= \frac{\sigma_1(x,\chi)}{\sigma_n(x,\chi)} \|B_{LL}^0 + D(x,\chi)\|_2^{-1}. \end{aligned} \tag{45}$$

Combining (42), (44), and (45), we have

$$\|Z\|_\infty \le \sqrt{n} \|Z\|_2 \le n \frac{\sigma_1(x,\chi)}{\sigma_n(x,\chi)} \|B_{LL}^0\|_\infty^{-1}. \tag{46}$$

Next, we show $\sigma_n(x,\chi) \ge \tau_n$. Since $B_{LL}(x,\chi)$ is a diagonally dominant symmetric matrix, and all its diagonal entries are negative, $B_{LL} \prec 0$ is negative definite. Therefore, $\sigma_n(x,\chi)$ is equal to the opposite of the largest eigenvalue of $B_{LL}(x,\chi)$. According to the Courant-Fischer theorem [21], we have

$$\begin{aligned} -\sigma_n(x,\chi) &= \max_{y \ne 0} \frac{y^{\mathrm{T}} \left(B_{LL}^0 + D(x,\chi)\right) y}{y^{\mathrm{T}} y} \\ &\le \max_{y \ne 0} \frac{y^{\mathrm{T}} B_{LL}^0 y}{y^{\mathrm{T}} y} + \max_{y \ne 0} \frac{y^{\mathrm{T}} D(x,\chi) y}{y^{\mathrm{T}} y}. \end{aligned} \tag{47}$$

Since $D(x,\chi) \preceq 0$, the quadratic form $y^{\mathrm{T}} D(x,\chi) y \le 0$, which implies

$$-\sigma_n(x,\chi) \le \max_{y \ne 0} \frac{y^{\mathrm{T}} B_{LL}^0 y}{y^{\mathrm{T}} y} = -\tau_n \Rightarrow \sigma_n(x,\chi) \ge \tau_n. \tag{48}$$

In the last step, we show $\sigma_1(x,\chi) \le \tau_1 - b$, where $b = \min\{b_i^G + b_i^C \mid i = 1, \ldots, n\} < 0$ is the lower bound of the diagonal entries of $D(x,\chi)$. Similar to the previous step, $\sigma_1(x,\chi)$ is equal to the opposite of the smallest eigenvalue of $B_{LL}(x,\chi)$ and

$$\begin{aligned} -\sigma_1(x,\chi) &= \min_{y \ne 0} \frac{y^{\mathrm{T}} \left(B_{LL}^0 + D(x,\chi)\right) y}{y^{\mathrm{T}} y} \\ &\ge \min_{y \ne 0} \frac{y^{\mathrm{T}} B_{LL}^0 y}{y^{\mathrm{T}} y} + \min_{y \ne 0} \frac{y^{\mathrm{T}} D(x,\chi) y}{y^{\mathrm{T}} y} \\ &\ge -\tau_1 + b. \end{aligned} \tag{49}$$

Then, we have

$$\sigma_1(x,\chi) \le \tau_1 - b. \tag{50}$$

Finally, combining (46), (48), and (50), we conclude

$$\max_{i,j}|Z_{ij}| \le \|Z\|_\infty \le \kappa \|B_{LL}^0\|_\infty^{-1},\ \kappa := n\frac{\tau_1 - b}{\tau_n}, \quad (51)$$

where κ is determined only by B_{LL}^0, independent of decision variables x and χ. □

C. Derivation of the Formula for M

From (10), two classes of constraints limit the value of M. When $z^{(k)} = 0$, we see $y^{(k)} = 0$ and require $M \ge \|W^{(k)}y^{(k-1)} + b^{(k)}\|_\infty$. When $z^{(k)} = 1$, we see $y^{(k)} = W^{(k)}y^{(k-1)} + b^{(k)}$ and require $M \ge \|y^{(k)}\|_\infty = \|W^{(k)}y^{(k-1)} + b^{(k)}\|_\infty$.

In summary, we require

$$M \ge \|W^{(k)}y^{(k-1)} + b^{(k)}\|_\infty,\ k = 1, \dots, K. \quad (52)$$

We give the following inequality to estimate the upper bound of $\|y^{(k)}\|_\infty$ and $\|W^{(k)}y^{(k-1)} + b^{(k)}\|_\infty$.

$$\begin{aligned}\|y^{(k)}\|_\infty &\le \|W^{(k)}y^{(k-1)} + b^{(k)}\|_\infty \\ &\le \|W^{(k)}\|_\infty \|y^{(k-1)}\|_\infty + \|b^{(k)}\|_\infty \\ &\le \|y^{(0)}\|_\infty \prod_{i=1}^{k}\|W^{(i)}\|_\infty \\ &\quad + \sum_{i=1}^{k}\|b^{(i)}\|_\infty \prod_{j=i+1}^{k}\|W^{(j)}\|_\infty, k = 1, \dots, K. \quad (53)\end{aligned}$$

Since $y^{(0)} = \begin{bmatrix} x \\ \chi \end{bmatrix}$ is composed of binary variables that are in the range of $\{0, 1\}$, we see $\|y^{(0)}\|_\infty \le 1$. Let

$$M_k := \prod_{i=1}^{k}\|W^{(i)}\|_\infty + \sum_{i=1}^{k}\|b^{(i)}\|_\infty \prod_{j=i+1}^{k}\|W^{(j)}\|_\infty. \quad (54)$$

Then, the value can be set as $M := \max_{1\le k\le K} M_k$.

D. Proof of Theorem 4

Proof: As derived in (17), the SCR γ can be calculated by

$$\gamma = \min\lambda(-B_r, P) = \min\lambda(-\sqrt{P}^{-1}B_r\sqrt{P}^{-1}), \quad (55)$$

where $\sqrt{P}^{-1}B_r\sqrt{P}^{-1}$ is symmetric. Suppose there is a perturbation δB_r on B_r, i.e., $\tilde{B}_r = B_r + \delta B_r$, then the perturbed SCR $\tilde{\gamma}$ can be evaluated by

$$\tilde{\gamma} = \gamma - \frac{y^{\mathrm{T}}\sqrt{P}^{-1}\delta B_r\sqrt{P}^{-1}y}{y^{\mathrm{T}}y} + o\left(\|\delta B_r\|_F^2\right), \quad (56)$$

where y is the eigenvector of $-\sqrt{P}^{-1}B_r\sqrt{P}^{-1}$ corresponding to γ. The detailed derivation of (56) can be found in [21].

Furthermore, it is easy to see the following inequality holds,

$$\begin{aligned}\left|\frac{y^{\mathrm{T}}\sqrt{P}^{-1}\delta B_r\sqrt{P}^{-1}y}{y^{\mathrm{T}}y}\right| &= \left|\frac{\sum_{i,j}\delta_{ij}y_iy_j\sqrt{P_iP_j}^{-1}}{y^{\mathrm{T}}y}\right| \\ &\le \frac{\sum_{i,j}\sqrt{P_iP_j}^{-1}|y_iy_j||\delta_{ij}|}{y^{\mathrm{T}}y} \\ &\le \frac{\sum_{i,j}\sqrt{P_iP_j}^{-1}|y_iy_j|}{y^{\mathrm{T}}y}\delta. \quad (57)\end{aligned}$$

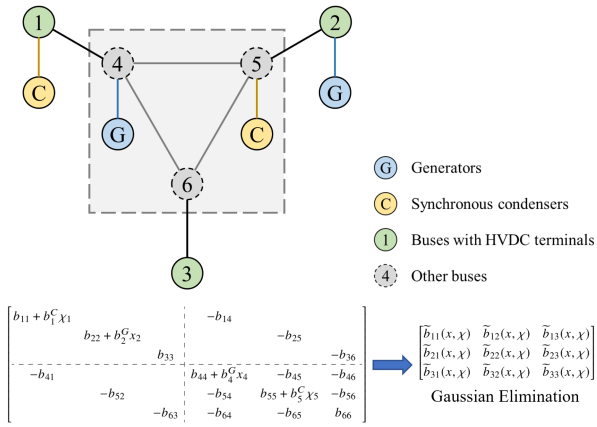

Fig. 7 A 6-bus system for illustrating the reduced admittance matrix B_r. Buses outside the gray area remain, and buses inside the gray area are aggregated.

It implies

$$\begin{aligned}|\tilde{\gamma} - \gamma| &\le \left|\frac{y^{\mathrm{T}}\sqrt{P}^{-1}\delta B_r\sqrt{P}^{-1}y}{y^{\mathrm{T}}y}\right| + o\left(\|\delta B_r\|_F^2\right) \\ &\le \frac{\sum_{i,j}\sqrt{P_iP_j}^{-1}|y_iy_j|}{y^{\mathrm{T}}y}\delta + o\left(\delta^2\right) \\ &=: C\delta + o\left(\delta^2\right). \quad (58)\end{aligned}$$

Therefore, the SCR error $|\tilde{\gamma} - \gamma|$ is bounded by the admittance error δ. □

E. An Example for Calculating B_r

We take a 6-bus system as an example to illustrate the calculation of the reduced admittance matrix B_r. The system network is shown in Fig. 7, where Bus #1, Bus #2, and Bus #3 are connected with HVDC terminals.

The admittance matrix of the system is denoted by

$$B(x, \chi) = \begin{bmatrix} B_{HH}(x, \chi) & B_{HL} \\ B_{LH} & B_{LL}(x, \chi) \end{bmatrix}, \quad (59)$$

where H indicates buses with HVDC terminals and L indicates other buses. In this example, H and L are $\{1, 2, 3\}$ and $\{4, 5, 6\}$, respectively. The detailed expression of $B(x, \chi)$ is given by

$$B_{HH}(x, \chi) = \begin{bmatrix} b_{11} + b_1^C\chi_1 & & \\ & b_{22} + b_2^Gx_2 & \\ & & b_{33} \end{bmatrix},$$

$$B_{HL} = \begin{bmatrix} -b_{14} & & \\ & -b_{25} & \\ & & -b_{36} \end{bmatrix} = B_{LH},$$

$$B_{LL}(x, \chi) = \begin{bmatrix} b_{44} + b_4^Gx_4 & -b_{45} & -b_{46} \\ -b_{54} & b_{55} + b_5^C\chi_5 & -b_{56} \\ -b_{64} & -b_{65} & b_{66} \end{bmatrix}. \quad (60)$$

In (60), b_{ij} represents the admittance of the (i,j) line, $b_{ii} = -\sum_{j\neq i} b_{ij}$, and b_i^G, b_i^C are the admittances of the corresponding generator and the synchronous condenser, respectively.

When we calculate the SCR, we need to obtain the reduced admittance matrix B_r. The formulation of B_r is given by

$$B_r(x,\chi) = B_{HH}(x,\chi) - B_{HL}B_{LL}(x,\chi)^{-1}B_{LH} = \begin{bmatrix} \widetilde{b}_{11}(x,\chi) & \widetilde{b}_{12}(x,\chi) & \widetilde{b}_{13}(x,\chi) \\ \widetilde{b}_{21}(x,\chi) & \widetilde{b}_{22}(x,\chi) & \widetilde{b}_{23}(x,\chi) \\ \widetilde{b}_{31}(x,\chi) & \widetilde{b}_{32}(x,\chi) & \widetilde{b}_{33}(x,\chi) \end{bmatrix}. \quad (61)$$

Mathematically, the reduced admittance matrix B_r just results from the Gaussian elimination of $B(x,\chi)$.

In Section III-A, we introduced an additional decision variable Z to represent the inverse of B_{LL}. Then, B_r can be equivalently obtained through

$$B_r = B_r(x,\chi,Z) = B_{HH}(x,\chi) - B_{HL}ZB_{LH}, \quad (62)$$

which implies that B_r is linear to x, χ and Z.

In Section III-B, we proposed a data-driven approach to approximate $\tilde{B} := B_{HL}B_{LL}(x,\chi)^{-1}B_{LH}$, and then, B_r can be approximated by

$$\tilde{B}_r = \tilde{B}_r(x,\chi,\tilde{B}) = B_{HH}(x,\chi) - \tilde{B}, \quad (63)$$

which also implies that $\tilde{B}_r$ is linear to x, χ and $\tilde{B}$.

REFERENCES

[1] A. Kalair, N. Abas, and N. Khan, "Comparative study of HVAC and HVDC transmission systems," *Renewable Sustain. Energy Rev.*, vol. 59, pp. 1653–1675, 2016. [Online]. Available: https://www.sciencedirect.com/science/article/pii/S1364032115016718

[2] A new energy network: HVDC development in China, 2022. [Online]. Available: http://cleanandsecuregrid.org/2017/01/02/a-new-energy-network-hvdc-development-in-china/

[3] Welcome to State Grid Corporation of China: UHV, 2022. [Online]. Available: http://www.sgcc.com.cn/html/sgcc_main_en/col2017112610/column_2017112610_1.shtml

[4] N. Zhang et al., "Data-driven security and stability rule in high renewable penetrated power system operation," *Proc. IEEE*, vol. 111, no. 7, pp. 788–805, Jul. 2023.

[5] M. Langwasser, G. De Carne, M. Liserre, and M. Biskoping, "Fault current estimation in multi-terminal HVDC grids considering MMC control," *IEEE Trans. Power Syst.*, vol. 34, no. 3, pp. 2179–2189, May 2019.

[6] C. Galvez and A. Abur, "Fault location in hybrid AC/DC transmission grids containing DERs and HVDC lines," *IEEE Trans. Power Syst.*, vol. 39, no. 1, pp. 329–340, Jan. 2024.

[7] P. Krishayya et al., "IEEE guide for planning dc links terminating at ac locations having low short-circuit capacities, Part I: AC/DC system interaction phenomena," *IEEE Std 1204-1997*, pp. 1–216, 1997, doi: 10.1109/IEEESTD.1997.85949.

[8] B. Davies et al., "System with multiple DC infeed," CIGRE, France, Tech. Rep. ELT_241_6, 2008. [Online]. Available: https://www.e-cigre.org/publications/detail/364-systems-with-multiple-dc-infeed.html

[9] F. Zhang, H. Xin, D. Wu, Z. Wang, and D. Gan, "Assessing strength of multi-infeed LCC-HVDC systems using generalized short-circuit ratio," *IEEE Trans. Power Syst.*, vol. 34, no. 1, pp. 467–480, Jan. 2019.

[10] X. Liu, H. Xin, D. Zheng, D. Chen, and J. Tu, "Transient stability of synchronous condenser co-located with renewable power plants," *IEEE Trans. Power Syst.*, vol. 39, no. 1, pp. 2030–2041, Jan. 2024.

[11] S. Teleke, T. Abdulahovic, T. Thiringer, and J. Svensson, "Dynamic performance comparison of synchronous condenser and SVC," *IEEE Trans. Power Del.*, vol. 23, no. 3, pp. 1606–1612, Jul. 2008.

[12] J. Jia, G. Yang, A. H. Nielsen, and V. Gevorgian, "Investigation on the combined effect of VSC-based sources and synchronous condensers under grid unbalanced faults," *IEEE Trans. Power Del.*, vol. 34, no. 5, pp. 1898–1908, Oct. 2019.

[13] S. Hadavi, D. B. Rathnayake, G. Jayasinghe, A. Mehrizi-Sani, and B. Bahrani, "A robust exciter controller design for synchronous condensers in weak grids," *IEEE Trans. Power Syst.*, vol. 37, no. 3, pp. 1857–1867, May 2022.

[14] Y. Zhang, D. Davis, and M. J. Brear, "Least-cost pathways to net-zero, coupled energy systems: A case study in Australia," *J. Cleaner Prod.*, vol. 392, 2023, Art. no. 136266. [Online]. Available: https://www.sciencedirect.com/science/article/pii/S0959652623004249

[15] A. Jindal and G. Shrimali, "Cost–benefit analysis of coal plant repurposing in developing countries: A case study of India," *Energy Policy*, vol. 164, 2022, Art. no. 112911. [Online]. Available: https://www.sciencedirect.com/science/article/pii/S0301421522001367

[16] L. Huang, H. Xin, Z. Li, P. Ju, H. Yuan, and G. Wang, "Identification of generalized short-circuit ratio for on-line stability monitoring of wind farms," *IEEE Trans. Power Syst.*, vol. 35, no. 4, pp. 3282–3285, Jul. 2020.

[17] Z. Chu and F. Teng, "Short circuit current constrained UC in high IBG-penetrated power systems," *IEEE Trans. Power Syst.*, vol. 36, no. 4, pp. 3776–3785, Jul. 2021.

[18] H. Yuan et al., "Assessing maximal capacity of grid-following converters with grid strength constraints," *IEEE Trans. Sustain. Energy*, vol. 13, no. 4, pp. 2119–2132, Oct. 2022. [Online]. Available: https://ieeexplore.ieee.org/document/9800140/

[19] S. Hadavi, J. Saunderson, A. Mehrizi-Sani, and B. Bahrani, "A planning method for synchronous condensers in weak grids using semi-definite optimization," *IEEE Trans. Power Syst.*, vol. 38, no. 2, pp. 1632–1641, Mar. 2023.

[20] Z. Chu and F. Teng, "Voltage stability constrained unit commitment in power systems with high penetration of inverter-based generators," *IEEE Trans. Power Syst.*, vol. 38, no. 2, pp. 1572–1582, Mar. 2023.

[21] G. W. Stewart and J. Sun, *Matrix Perturbation Theory*. New York, NY, USA: Academic, 1990.

[22] Z. Zhuo et al., "Cost increase in the electricity supply to achieve carbon neutrality in China," *Nature Commun.*, vol. 13, no. 1, Jun. 2022, Art. no. 3172. [Online]. Available: https://doi.org/10.1038/s41467-022-30747-0

[23] Z. Zhuo et al., "Transmission expansion planning test system for AC/DC hybrid grid with high variable renewable energy penetration," *IEEE Trans. Power Syst.*, vol. 35, no. 4, pp. 2597–2608, Jul. 2020.

[24] J. Yang, N. Zhang, C. Kang, and Q. Xia, "A state-independent linear power flow model with accurate estimation of voltage magnitude," *IEEE Trans. Power Syst.*, vol. 32, no. 5, pp. 3607–3617, Sep. 2017. [Online]. Available: https://ieeexplore.ieee.org/document/7782382/

[25] H. Jia et al., "Voltage stability constrained operation optimization: An ensemble sparse oblique regression tree method," *IEEE Trans. Power Syst.*, vol. 39, no. 1, pp. 160–171, Jan. 2024.

[26] R. Jabr, "Radial distribution load flow using conic programming," *IEEE Trans. Power Syst.*, vol. 21, no. 3, pp. 1458–1459, Aug. 2006.

[27] J. Lavaei and S. H. Low, "Zero duality gap in optimal power flow problem," *IEEE Trans. Power Syst.*, vol. 27, no. 1, pp. 92–107, Feb. 2012.

[28] Y. Chen et al., "Security-constrained unit commitment for electricity market: Modeling, solution methods, and future challenges," *IEEE Trans. Power Syst.*, vol. 38, no. 5, pp. 4668–4681, Sep. 2023.

[29] *Gurobi Optimization, LLC*, "Gurobi optimizer reference manual," 2023. [Online]. Available: https://www.gurobi.com

[30] M. ApS, "The MOSEK optimization toolbox for MATLAB manual. version 10.0," 2022. [Online]. Available: http://docs.mosek.com/9.0/toolbox/index.html

[31] B. Cui and X. A. Sun, "A new voltage stability-constrained optimal power-flow model: Sufficient condition, SOCP representation, and relaxation," *IEEE Trans. Power Syst.*, vol. 33, no. 5, pp. 5092–5102, Sep. 2018.

Jiaxin Wang (Graduate Student Member, IEEE) received the B.S. degree in electrical engineering in 2022 from Tsinghua University, Beijing, China, where he is currently working toward the Ph.D. degree. His research interests include power system operation and planning, stability constrained optimization, and machine learning in power systems.

Jiawei Zhang (Graduate Student Member, IEEE) received the B.S. degree in mathematics and physics with a minor in computer science in 2019 from Tsinghua University, Beijing, China, where he is currently working toward the Ph.D. degree of electrical engineering. His research focuses on power system operation, planning, and frequency stability.

Qingchun Hou (Member, IEEE) received the B.S. degree from the Huazhong University of Science and Technology, Wuhan, China, in 2016, and the Ph.D. degree from Tsinghua University, Beijing, China, in 2021. He is currently an Algorithm Expert with Alibaba. His research interests include power system operation and planning with high renewable energy penetration, data-driven analytics, power system optimization, and machine learning. He was the recipient of the Advanced Technology Talent Program "AliStar" of Alibaba.

Ning Zhang (Senior Member, IEEE) received the B.S. and Ph.D. degrees from Tsinghua University, Beijing, China, in 2007 and 2012, respectively. He is currently an Associate Professor with Tsinghua University. His research interests include power system planning and operation under renewable energy penetration and multiple energy systems integration.